Supplementary information

Michael Mercer, Chao Peng, Cindy Soares, Harry Hoster and Denis Kramer

October 23, 2020

1 Supplemental DFT calculations

1.1 Input unit cells in cluster expansions (CE)

In Figure S1, the unit cells that were input into the cluster expansion, shown in the main paper, are represented. The lattice parameters are shown in Table S1.

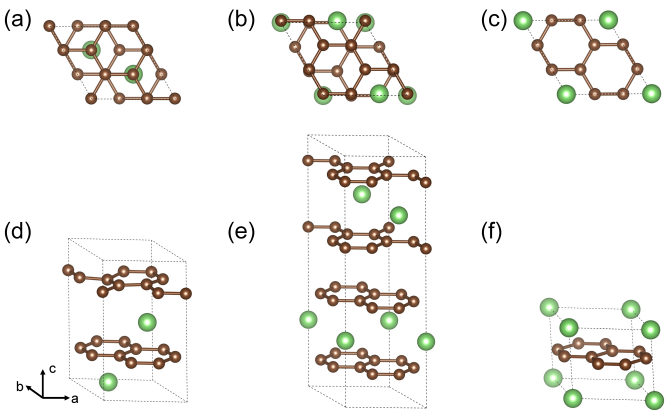

Figure S1: Unit cells used in cluster expansions for (a,d) AB stacked graphite, (b,e) AABB stacked graphite, (c,f) AA stacked graphite.The green balls represent Li atoms while the brown-colored balls indicate C atoms. These notations are used throughout this work.

Table S1: Lattice parameters of the unit cells for different graphite stacking.

Graphite stacking	Lattice constants
AB	$a = b = 4.31$ Å, $c = 7.55$ Å; $\alpha = \beta = 90°$, $\gamma = 120°$
AABB	$a = b = 4.32$ Å, $c = 14.01$ Å; $\alpha = \beta = 90°$, $\gamma = 120°$
AA	$a = b = 4.32$ Å, $c = 3.70$ Å; $\alpha = \beta = 90°$, $\gamma = 120°$

1.2 Climbing image nudged elastic band calculations

Based on the ground state structures found from the cluster expansion as shown in the main paper, activation energies for transitions between different carbon stackings were evaluated through the climbing image nudged elastic band (CI-NEB) method [1;2]. This section provides more information about these energy landscapes as a function of Li content. The layer transitions are represented in Figure S2. CI-NEB results, showing how the energy of the system evolves as those structural motifs are translated are shown in Figure S3.

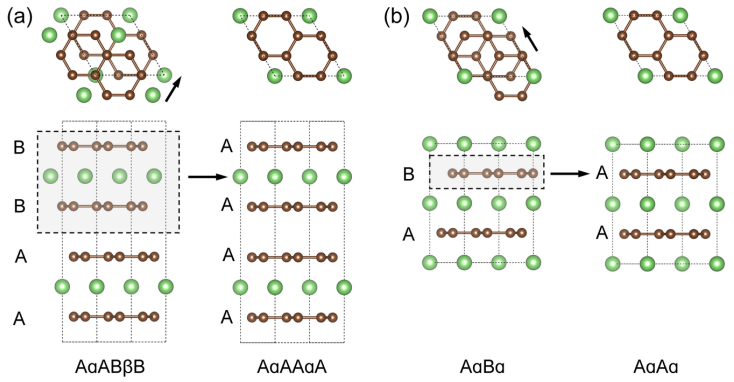

Figure S2: Translation of carbon layer stacking in (a) graphite with $x = 0.5(LiC_{12})$, representing the shift between dilute Stage II and Stage II, (b) graphite with $x = 1$ (LiC_6). The dashed rectangles indicate the structural motifs that translate during the layer shifting. The directions of the layer shifts are also represented in the top down views.

Figure S3a-e show the energy profiles associated with a change in stacking at different Li fraction of Li_xC_6 (x = 0, 0.17, 0.41, 0.5 and 1.0) based on the identified ground states in the main paper.

With $x = 0$, there is an energy barrier of 82.45 meV/6C for the graphene layer shifting from AB stacking to AA stacking in graphite (Figure S3b). AB stacking results in a local energy minimum while AA stacked graphite is the energetically maximum state. This confirms AB stacking in the host lattice is favourable at $x = 0$. When $x = 0.17$, AA stacked graphite is still the maximum energy state, but AABB is more favourable than ABAB. An energy barrier of 42.95 meV/6C is required for the structure shift from AABB to AAAA stacking (Figure S3c).

With $x = 0.41$, our calculations revealed the most stable structure to assume neither AABB nor AA stacking, but rather structures with the carbon atoms in between these stacking configurations, i.e. intermediate states (IS). The structure needs to overcome barriers to shift from the IS to either the AαABαB or AαAAαA stackings. Based on the depth of the well of the black line in Figure S3c, we quantify a barrier of 6.89 meV/6C to transfer from the intermediate states to an AαAAαA stacked configuration. These intermediate states were also verified by the potential energy surface calculations as shown in Figure S3f, with "intermediate" states indicated by the red minima.

When $0.5 < x < 1$, AαBα is the energetic maximum while AαAα is the

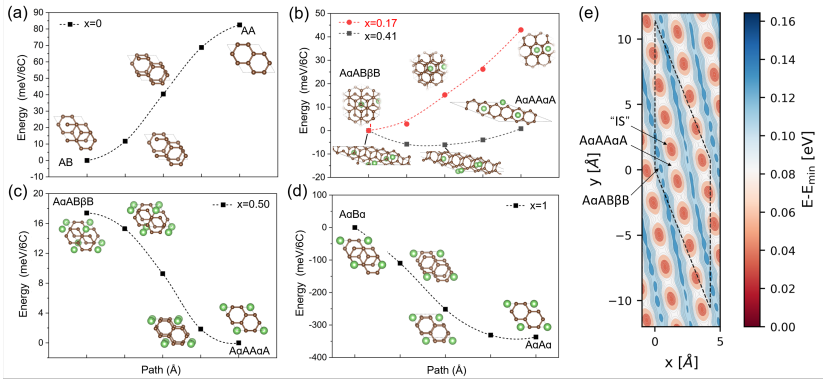

Figure S3: Energy profiles of stacking changes from CI-NEB methods are shown for (a): AB to AA carbon stacking for $x = 0$; (b-c): AαABβB stacking for $0.17 \leq x \leq 0.50$; (d): AαAα to AαBα for $x = 1$. Top-down structural representations of the unit cells along the CI-NEB path are shown. (e): Two dimensional potential energy surface representing motion of a BβB motif over a fixed AαA unit, in the AABB stacked system at $x = 0.41$ (b, black line represents a line profile of the same situation). The coloured bar indicates the energy difference between the intermediate states (IS) and other sampled structures.

minimum. Therefore, there is no barrier to shift from AαBα to AαAα, confirming that the host lattice structure displays AA stacking in Stages I and II (Figure S3d-e).

During lithiation from $x = 0.17$, the shift from AABB to AAAA is not feasible because of a high energy barrier of 42.95 meV/6C (Figure S3b). Thus the stacking shift occurs for $x > 0.17$. Similarly, in the reverse delithiation direction translation from AAAA to AABB is not feasible until $x < 0.5$ because of the high energy required for this structural shift of about 17.18 meV/6C (Figure S3c).

We find that there is a smooth monotonous path connecting the ground state stacking to possible alternative stackings. In the case of the intermediate state (IS), there is an energy minimum for carbon layers in configurations between AAAA and AABB stackings. However, this behaviour does not explain the hysteresis, since the lattice could simply follow the minimum energy configuration in both directions without any uphill energetic barrier. Therefore, energetic barriers to transition between carbon stackings based purely on ground state configurations do not explain the hysteresis.

As explored in the CI-NEB section in the main paper, just considering ground state Li configurations in these transitions may be a simplification. It would increase the configurational entropy of the system to introduce Li in the interplane of Stage II configurations at $x = 0.5$ and our experimental analysis suggests that these configurations are indeed accessed. Hence we find the presence of interplanar sites, rather than intrinsic barriers to transition between carbon stacking with Li in ground state configurations, is important to explaining the hysteresis effect.

In the subsequent section, we present further details on how the entropy profiling measurements were performed, analysed and post processed to infer

information about the interplanar Li concentrations. Additionally we describe the calculation to approximate the vibrational entropy dependent on x.

1.3 Details of cluster expansion

To sample the Li orderings in the Li/graphite system, we carried out the cluster expansion method within the Alloy Theoretic Automated Toolkit (ATAT) package to describe the energies of different configurations based on the Ising model[3;4]. This method has previously been successfully applied in the Li/graphite system to compute Li orderings and diffusion[5;6]. The lattice site is denoted by occupation variables, which take values +1 if occupied by Li and is -1 when the site is vacant. Li ordering is allowed to change in three dimensional (3D) directions. The AB stacked cluster expansion was fitted to the energies of 58 Li-vacancy configurations, and 126 Li-vacancy configurations were sampled in AABB stacked graphite. For AA stacked graphite, 87 Li-vacancy configurations were fitted by the cluster expansion. The evaluation of the predicted energies of structures by cluster expansion relative to the DFT energies is described by the weighted cross-validation score that were 3.5, 9.2 and 5.2 meV/6C for AB, AABB and AA stacked graphite, respectively.

2 Extra entropy and enthalpy profile analysis

In this section we present further analysis of the experimental entropy and enthalpy profiles presented in the main paper. The experimental protocols that were summarised in the main paper are also described here in more detail.

2.1 Experimental protocols

All entropy profiling measurements described subsequently were preceded by a constant current/constant voltage (dis)charging protocol, designated "CCCV (dis)charge", to ensure a consistent starting lithiation state for each experiment. A CCCV charge consists of galvanostatic delithiation at C/20 (18.6 mA/g) up to 1.5 V, followed by at least 2 hours of polarisation at 1.5 V. A CCCV discharge starts with galvanostatic lithiation at C/25 (14.88 mA/g) down to 0.005 V, followed by at least 2 hours of polarisation at 0.005 V. The low C-rate here was designed to mitigate the risk of lithium plating so close to 0 V, while allowing lithiation as close as possible to the ideal LiC_6 structure ($x = 1$).

Entropy profiling in lithiation mode was performed in an iterative procedure, where the current and temperature were changed dynamically as outlined in Table S2. The central temperature, T_c was varied as indicated in the results section. Entropy measurements comprising iterative steps of galvanostatic discharge were initiated by performing a "CCCV charge" step at $T = T_c + 3\,^{\circ}\mathrm{C}$. Each iteration was repeated until the cell voltage was less than 0.005 V, mirroring the cutoff voltage of the CCCV discharge procedure. State of charge, x, was obtained from normalising the change of capacity from each galvanostatic step in Table S2 to the total change of capacity obtained during the entire experiment.

We also performed a set of measurements where profiles were initiated from a "CCCV discharge" at $T = T_c + 3\,^{\circ}\mathrm{C}$, and the graphite electrode was delithiated

stepwise at C/25. These experiments were cut off once the cell voltage reached a value greater than 1.5 V. The temperature program in Table S2 was also used here, except that step 1 was a charge rather than a discharge.

Step	**Time (min)**	**Temperature T (°C)**	**Applied T at $T_c = 25$ °C**
Discharge (C/25)	20	$T_c + 3$	28
OCV relaxation	20	$T_c + 3$	28
Temperature step T_1 at OC	20	T_c	25
Temperature step T_2 at OC	20	$T_c - 3$	22
Temperature step T_3 at OC	20	$T_c + 3$	28

Table S2: Conditions applied during each iteration of the entropy profiling experiments. An example temperature profile at $T_c = 25$ °C is illustrated for clarity in the right hand column.

2.2 Partial molar entropy contributions

It is known that not only configurational, but also vibrational entropy contributes to measured entropy profiles, i.e.

$$\frac{\partial S}{\partial x} = \frac{\partial S_{config}}{\partial x} + \frac{\partial S_{vib}}{\partial x} + \frac{\partial S_{electronic}}{\partial x} \tag{S1}$$

where S, S_{config}, S_{vib}, $S_{electronic}$ are the total, configurational, vibrational and electronic entropy, respectively [7;8]. Note that as graphite is a semimetal, with a low density of states at the Fermi level we will neglect the electronic contribution, similar to assumptions presented earlier by Reynier et al. [8]. The term with the most significant effect on the entropy is the configurational term, which we have modelled in our previous work [9]. This is responsible for the step in the entropy profile at $x = 0.5$, the order/disorder transition [7;9]. It is also responsible for the transition (to a very good approximation) to solid solution behaviour for $x < 0.5$.

We found an unexpected slope in the derived entropy profiles in the region $0.5 < x < 1$ (x = fraction of Li in LiC_6). This slope has been observed in other entropy profile results but has so far not been explained. This is a puzzling result because it would be expected that the partial molar (p.m.) entropy in the Stage I - Stage II region, which shows two phase coexistence, would not show any variation with composition within the usual common tangent construction of the thermodynamic variables $G(x)$, $H(x)$ and $S(x)$ across a two phase region.

2.3 Analysis of the vibrational term

The vibrational term in equation S1 is significant. The more comprehensive attempt so far to quantify the effect of vibrational entropy due to lithium insertion in graphite was made by Reynier, Yazami and Fultz [7]. The vibrational entropy depends on all phonon frequencies of the solid, but it is common to extract a Debye temperature from measured phonon spectra, which can be obtained from inelastic neutron scattering experiments [10;11;12]. A Debye temperature is a convenient but approximate parameterization for the phonon energy spectrum [7].

Although vibrational entropy is smaller effect than configurational entropy in the solid solution regions, it does result in a quantitative contribution to the overall entropy profile[7;8]. Previously, Reynier et al. assumed the partial molar vibrational entropy to be a constant correction factor that does not vary with x[7]. Only the contribution in the interval $0.5 < x < 1$ was explicitly considered, but we will discuss more dilute compositions shortly. For these compositions, Reynier et et al. utilised the approximation

$$\frac{\partial S_{vib}}{\partial x} = R \ln\left(\frac{\Theta_{D0}}{\Theta_{D\perp}}\right) + 2R \ln\left(\frac{\Theta_{D0}}{\Theta_{D\parallel}}\right) \tag{S2}$$

where S_{vib} is the vibrational entropy, R is the molar gas constant, Θ_{D0} is the Debye temperature of bcc metallic lithium, $\Theta_{D\parallel}$ and $\Theta_{D\perp}$ are the Debye temperatures for lithium vibrations parallel and perpendicular to the graphene planes, respectively.

Equation S2 can be interpreted physically as follows. As x increases we extract one lithium atom from the metallic lithium anode and another lithium is intercalated into the graphite (the cathode in half cell experiments). The resultant entropy change measured during entropy profiling is therefore the difference between the cathode and anode contribution

$$\frac{\partial S}{\partial x} = \frac{\partial S_{cathode}}{\partial x} - \frac{\partial S_{anode}}{\partial x} \tag{S3}$$

where $S_{cathode}$ and S_{anode} are the respective entropy contributions from the cathode and anode. In the balance of equation S3 the configurational term from the anode can be neglected, since it is a metal with an entropy change of zero.

The vibrational entropy of lithium in graphite is determined by two modes of lithium vibrating parallel to the graphene planes (two degrees of freedom) plus one perpendicular vibrational mode. Since we consider entropy changes with respect to lithium being inserted or removed from the cathode, we neglect vibrational modes associated with the carbon host. The lithium atoms in the bcc metallic lithium anode has three vibrational modes which are the same in all 3 dimensions by symmetry. Thus applying equation S3 and assigning a Debye temperature to each mode we arrive at equation S2.

Reynier et al. considered that the vibrational entropy for all Li-graphite stages is the same, based on parameters for the Debye temperatures from Moreh et al.[7;11]. This is a good first approximation and is physically reasonable for Stages I and II, which both assume $\sqrt{3}$ by $\sqrt{3}$ stacking in the Li occupied layers, and within a nearest neighbour picture, have the same environment around each Li atom. This then leads to a constant background correction for all x. For this first approximation, Reynier et al. used Θ_{D0} = 380 K[10], $\Theta_{D\parallel}$ = 392 K[11], $\Theta_{D\perp}$ = 892 K[11], leading to a correction ∂S_{vib} / ∂x = -8.18 J mol^{-1} K^{-1}. In terms of the scale used in the main paper this is equivalent to $T\partial S_{vib}$ / ∂x = -27.1 meV per C_6 formula unit at T = 320 K.

However, a follow up study by Schimer et al. suggested a different effective temperature $T_{D\parallel}$, and hence Debye temperature $\Theta_{D\parallel}$ in Stages I, II and a stage denoted 'LiC_{16}', ostensibly dilute Stage II (IID)[12]. They quoted values of effective temperature of $T_{D\parallel}$ = 147 K, 124 K and 120 K, respectively for stages I, II and IID. Using the 0 K approximation $\Theta_{D\parallel} = \frac{8}{3}T_{D\parallel}$[12], we obtain

Debye temperatures for Li vibration parallel to the graphene planes of 392 K, 330 K and 320 K, respectively for stages I, II and IID. No further study of the perpendicular Debye temperature has been performed since so we assume the same parameters as Reynier et al. for the other vibrational modes. The difference between the vibrational entropy change associated with Stages I and II is significant (-27.1 meV per C_6 versus -16.9 meV per C_6, at $T = 320$ K) and this is illustrated graphically below.

2.4 Results: Li-graphite stage vibrational entropy

Figure S4 shows an entropy profile obtained during discharge, as presented in the main paper. The constant Debye temperature approximation to the vibrational entropy change proposed by Reynier et al. is overlaid with the improved approximation using the parameters from Schirmer et al.[12]. The latter assumption leads to correction that varies almost linearly for all x, with a slight inflection at $x = 0.5$. We assumed a stoichiometry for Stage IID of LiC_{18} (x =0.33) but the result is insensitive to x within the range of reported values of x in Stage IID. We compare these values with the experimental entropy profile result obtained during lithiation at $T = 47\,^oC$ as reported in the main paper. The experimental profile obtained after subtracting the improved approximation to the vibrational entropy is overlaid for comparison.

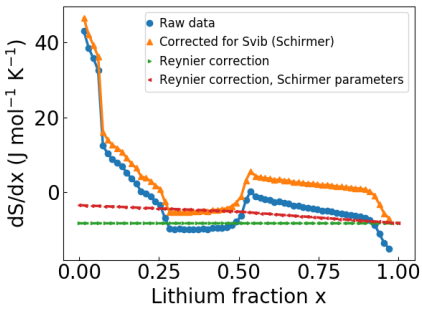

Figure S4: Entropy profile obtained during discharge, conducted at central temperature $T = 320$ K (raw data). The green dashed line shows the constant vibrational contribution assumed by Reynier et al.. Within the same assumption, but with the use of more recent parameters for the Debye temperatures, an improved correction can be obtained which accounts for changes in Debye temperature across different stages (red dashed line). Subtracting this latter correction from the raw data leads to the orange line: our best approximation to the entropy profile without any vibrational contributions. The resulting profile is predominantly determined by configurational entropy.

This analysis partly explains the origin of the observed slope in the entropy profile for $0.5 < x < 1$. The vibrational component no longer constant with x due to a a difference in the parameters describing the vibrational entropy in Stages I, II and IID. Although the phonon spectra and hence vibrational entropy of the higher order stages are not available to our knowledge, for now we extrapolate the vibrational entropy change of Stages II - Stage IID to lower

x.

The subtracted entropy profile crosses the point at $x = 0.5$ with $\partial S \,/\, \partial x \approx 0$, as we expect from simulated entropy profiles from lattice gas models of lithium intercalation in systems showing order/disorder transitions like graphite[9] and lithium manganese oxide[13;14], assuming only configurational entropy. This indicates that the quantitative magnitude of the vibrational correction is correct, and that we have successfully obtained only the configurational component to the p.m. entropy.

There still appears to be some varation in p.m. entropy values with x in the Stage I -Stage II two phase region, even after accounting for the vibrational entropy. This may be related to the Debye approximation, which approximates the entire phonon spectrum with a single Debye temperature. It is possible there is also a very small contribution from electronic entropy, but these effects are negligible and beyond the scope of the present work to examine further. Nevertheless, this is still a substantially improved description of the vibrational entropy of lithium in graphite and allows us to obtain only the configurational contribution. This enabled us to determine the configurational entropy as presented in the main paper.

2.5 Determination of interlayer Li concentration

The configuration entropy, S_{config} values as a function of x were evaluated from analysis of experimental profiles and presented in the main paper. Here it is shown how the S_{config} can be related to the interlayer concentrations n_1 and n_2, where $(n_1 + n_2)/2 = x$, within the assumption that two layers are filled.

Firstly we recall the well known result for the configurational entropy of an ideal solid solution. In this particular case, it means that $n_1 = n_2$.

$$S_{\text{config}}(x) = -R\left(x \log x + (1-x)\log(1-x)\right), \tag{S4}$$

and we also make use of the partial molar entropy

$$dS_{\text{config}}(x)/dx = -R\left(\log(x) - \log(1-x)\right). \tag{S5}$$

We also make note of the case where there is a large energy barrier between levels n_1 and n_2, which means that the level n_1 fills first as a solid solution until $x = 0.5$, then n_2 fills likewise. For $x < 0.5$, this is

$$S_{\text{config}}(x) = -\frac{R}{2}\left(2x \log\left(2x\right) + (1-2x)\log(1-2x)\right), \tag{S6}$$

leading to partial molar entropy

$$dS_{\text{config}}(x)/dx = -R\left(\log\left(2x\right) - \log(1-2x)\right), \tag{S7}$$

while for $x \geq 0.5$

$$S_{\text{config}}(x) = -\frac{R}{2}\left((2-2x)\log\left(2-2x\right) + (2x-1)\log(2x-1)\right), \tag{S8}$$

which leads to partial molar entropy

$$dS_{\text{config}}(x)/dx = -R\left(\log(2x-1) - \log(2-2x)\right). \tag{S9}$$

We now introduce the notation $n_1' = 1 - n_1$ and $n_2' = 1 - n_2$. In the general case, which is a good approximation to the $S_{\text{config}}(x)$ derived from the experimental data, the configurational entropy can be simply derived from Boltzmann's entropy equation and written as

$$S_{\text{config}}(n_1, n_2) = -\frac{R}{2}\left(n_1 \log n_1 + n_2 \log n_2 + n_1' \log n_1' + n_2' \log n_2'\right). \quad \text{(S10)}$$

It can be seen that equation S10 reduces to equation S4 when $n_1 = n_2$, as expected for the ideal solid solution. This means that the general two level configurational entropy at a given x has two unique solutions. However, these are the same but with n_1 and n_2 interchanged, so we take $n_1 > n_2$. So through a numerical procedure, we can determine n_1 and n_2 for a given known value of $S_{config}(x)$. This was achieved by inputting trial values of n_2, with starting values $n_2 = 0$ and $n_2 = n_1 = x$, and solving by an interval bisection method until the difference between the determined and true $S_{config}(x)$ was less than 10^{-6}.

References

[1] G. Henkelman and H. Jónsson, *The Journal of Chemical Physics*, 2000, **113**, 9978–9985.

[2] G. Henkelman, B. P. Uberuaga and H. Jónsson, *The Journal of Chemical Physics*, 2000, **113**, 9901–9904.

[3] A. van de Walle, M. D. Asta and G. Ceder, *Calphad*, 2002, **26**, 539–553.

[4] A. van de Walle, *Calphad*, 2009, **33**, 266–278.

[5] K. Persson, Y. Hinuma, Y. S. Meng, A. Van der Ven and G. Ceder, *Physical Review B*, 2010, **82**, 125416.

[6] K. Persson, V. A. Sethuraman, L. J. Hardwick, Y. Hinuma, Y. S. Meng, A. Van Der Ven, V. Srinivasan, R. Kostecki and G. Ceder, *The journal of physical chemistry letters*, 2010, **1**, 1176–1180.

[7] Y. Reynier, R. Yazami and B. Fultz, *Journal of Power Sources*, 2003, **119-121**, 850 – 855.

[8] Y. Reynier, J. Graetz, T. Swan-Wood, P. Rez, R. Yazami and B. Fultz, *Phys. Rev. B*, 2004, **70**, 174304.

[9] M. P. Mercer, M. Otero, M. Ferrer-Huerta, A. Sigal, D. E. Barraco, H. E. Hoster and E. P. Leiva, *Electrochimica Acta*, 2019, **324**, 134774.

[10] M. M. Beg and M. Nielsen, *Phys. Rev. B*, 1976, **14**, 4266–4273.

[11] R. Moreh, N. Shnieg and H. Zabel, *Phys. Rev. B*, 1991, **44**, 1311–1317.

[12] A. Schirmer, J. E. Fischer, P. Heitjans, H. J. Kim, A. Magerl, D. Vaknin and H. Zabel, *Molecular Crystals and Liquid Crystals Science and Technology. Section A. Molecular Crystals and Liquid Crystals*, 1994, **244**, 299–305.

[13] S. Schlueter, R. Genieser, D. Richards, H. E. Hoster and M. P. Mercer, *Phys. Chem. Chem. Phys.*, 2018, **20**, 21417–21429.

[14] M. P. Mercer, S. Finnigan, D. Kramer, D. Richards and H. E. Hoster, *Electrochimica Acta*, 2017, **241**, 141 – 152.